

Magnetic Nanostructures

U. Rücker

This document has been published in

Thomas Brückel, Gernot Heger, Dieter Richter, Georg Roth and Reiner Zorn (Eds.):
Lectures of the JCNS Laboratory Course held at Forschungszentrum Jülich and the
research reactor FRM II of TU Munich

In cooperation with RWTH Aachen and University of Münster

Schriften des Forschungszentrums Jülich / Reihe Schlüsseltechnologien / Key Tech-
nologies, Vol. 39

JCNS, RWTH Aachen, University of Münster

Forschungszentrum Jülich GmbH, 52425 Jülich, Germany, 2012

ISBN: 978-3-89336-789-4

All rights reserved.

10 Magnetic Nanostructures

U. Rücker

Jülich Centre for Neutron Science 2

Forschungszentrum Jülich GmbH

Contents

10.1	Introduction	2
10.2	Why neutrons are useful for investigating magnetic nanostructures	5
10.3	Specular reflectivity of polarized neutrons.....	6
10.4	Layer-by-layer magnetometry	9
10.5	Vector magnetometry	11
	References	19
	Exercises	20

10.1 Introduction

The physical properties of a layered structure of nanometer size, as it is shown schematically in Fig. 10.1, differs from the bulk properties of the constituents. There are several origins of new effects due to miniaturization:

The ratio between surface and volume is much higher than in bulk. Therefore, the amount of atoms with reduced coordination is significant and can change the crystalline structure as well as the electronic structure of the whole layer. Boundary conditions, e.g. for the magnetic induction \mathbf{B} become important, introducing shape anisotropies. The magnetization tends to align along the long edges of the magnetic nanostructure because the dipolar fields are smaller then.

At the interface between two layers, the electronic structures and the crystal lattices have to be matched, which leads to structural stress, interfacial disorder and electronically to charge transfer (e.g. a Shottky barrier in semiconductor heterostructures) or splitting of the layers' bandstructures.

Nanostructures can be prepared in several dimensions: thin films with a thickness in the nm range are 2D nanostructures, stripes with thickness and width in the nm range are 1D nanostructures and dots or nanoparticles with all three dimensions in the nm range are 0D nanostructures. The dimension number indicates, in how many directions the dimension remains macroscopic.

Magnetic nanostructures are nanostructures which contain at least one magnetic constituent. Typical systems are layered structures with ferromagnetic and nonmagnetic layers or arrays of ferromagnetic dots on a nonmagnetic substrate. The interesting aspect of magnetic nanostructures is the fact that two ferromagnetic (FM) layers with a nonmagnetic (NM) spacer in between have a connection between their electronic systems across the spacer layer. This connection influences as well the magnetic behaviour as the electron transport through the system.

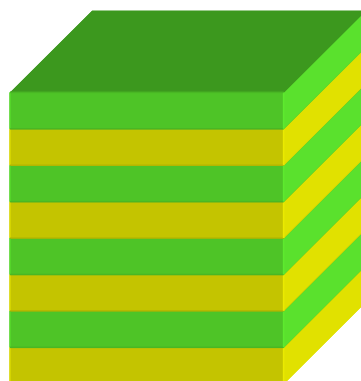


Fig. 10.1: *Sketch of a layered structure of two materials*

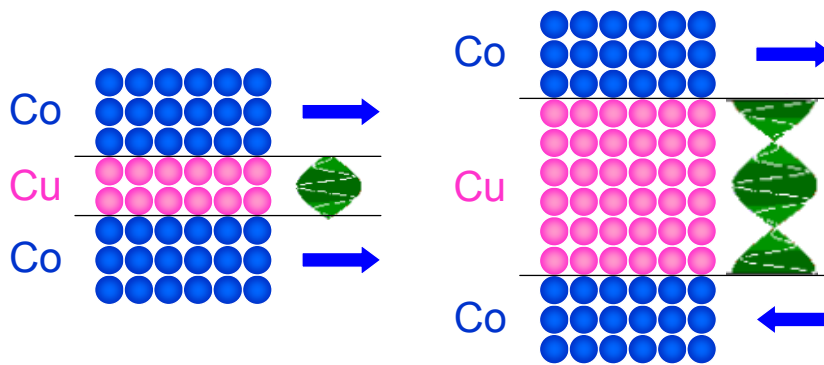


Fig. 10.2: *Oscillating interlayer coupling as a function of interlayer thickness*

The first phenomenon found in magnetic layered structures has been the oscillating magnetic interlayer coupling in FM / NM / FM trilayer structures. Depending on the NM interlayer thickness, the magnetizations of the two FM layers tend to align parallel or antiparallel to each other [1]. It turned out that the coupling is mediated by electronic states in the NM interlayer close to the Fermi surface [2]. The oscillation period of the coupling is related to the length of the wavevector of the electrons at the Fermi surface, as is sketched in Fig. 10.2.

Subsequently, the most important discovery followed, the Giant Magnetoresistance Effect (GMR) [3] [4]. For this discovery, P. Grünberg and A. Fert were honoured with the Nobel Prize for Physics 2007. They have found out that the resistivity of a layered structure containing more than one ferromagnetic layer depends on the mutual orientation of the magnetization directions, see Fig. 10.3. They used the antiferromagnetic coupling in Fe / Cr / Fe trilayer structures to be able to influence the mutual orientation of the magnetization of the Fe layers by changing the applied magnetic field.

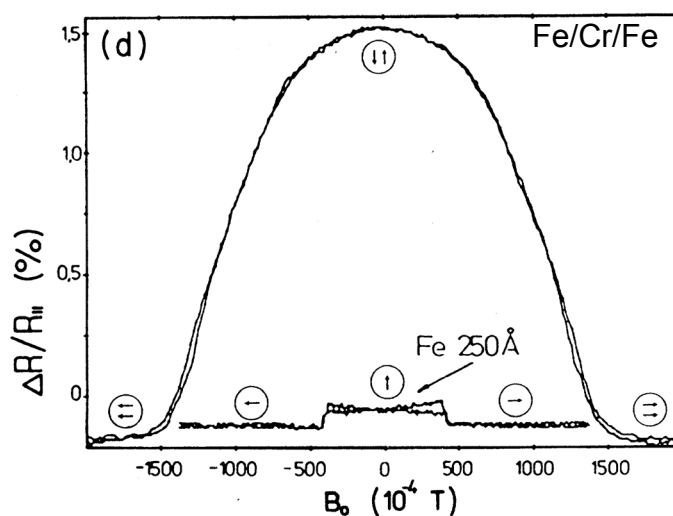


Fig. 10.3: *Giant Magnetoresistance effect in an Fe / Cr / Fe trilayer compared to the anisotropic magnetoresistance effect in a single Fe layer [3]*

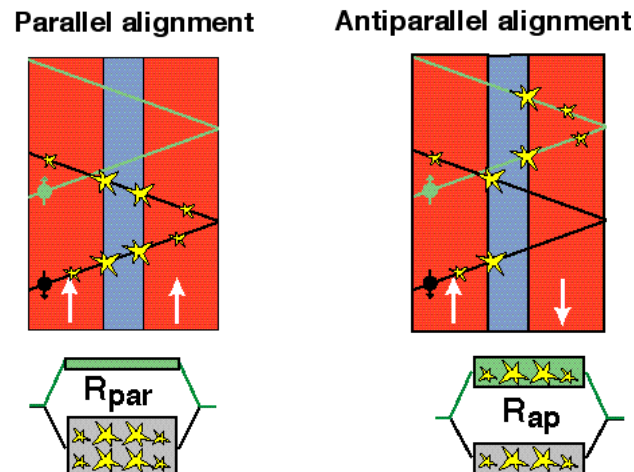


Fig. 10.4: *Different matching of the bandstructure between ferromagnetic and non-magnetic layers changes the resistivity for the different spin channels*

It turns out that the resistivity is highest in the case of antiparallel alignment of the two magnetization directions. This effect is much stronger and much more sensitive to changes in the magnetization direction of each ferromagnetic layer than the anisotropic magnetoresistance effect in single ferromagnetic layers, which was known before. The microscopic origin of the GMR effect is the matching between the spin-split bandstructures of the two ferromagnetic layers. The conductivity of the entire structure is the sum of the conductivities for the two spin channels. As the Fermi surface is different for the two spin channels, the matching between the FM and the NM layer is different.

As shown in Fig. 10.4, in the case of parallel alignment, the scattering probability of a conduction electron is the same at both interfaces. For one spin channel, the scattering probability is high while for the other it is low. The conductivity is then dominated by the spin channel with the smaller scattering probability. The resistivity of the entire structure, which can be described as a parallel wiring of the two resistors for the two spin channels, is small.

In the case of antiparallel alignment, the scattering probability for each spin channel is high in one of the FM layers. This results in a relatively low conductivity for both spin channel, so that the resulting resistivity is much higher compared to the case of parallel magnetization.

As GMR structures are easy to prepare and easy to use, the sensor technology based on this effect quickly became standard in the readout system of computer harddisks and many other applications. Today, it has been replaced by Tunneling Magnetoresistance (TMR), where the nonmagnetic interlayer is insulating and electrons travel across this tunneling barrier while preserving their spin state. Then, the height of the tunneling barrier depends on the spin of the electron and the magnetization direction of both ferromagnetic layers. A detailed overview over the field of spin transport in layered systems is given in Ref. [5].

10.2 Why neutrons are useful for investigating magnetic nanostructures

For the investigation of magnetism, many methods are well known. In most cases the magnetization of a sample is measured. A different, but more indirect approach is the measurement of spin-dependent bandstructures by absorption and photoemission spectroscopy of polarized light / x-rays.

The first (and oldest) approach is to measure the integral magnetization of a sample by classical magnetometry, e.g. by using a Vibrating Sample Magnetometer (which measures the induction when moving the magnetic sample in a coil), a Faraday balance (which measures the force on the magnetic sample in a field gradient), or more recently a SQUID magnetometer (which measures the magnetic flux inside a superconducting loop). In case of magnetic nanostructures, the small signal coming from the nanostructure is always superimposed by the signal from the substrate which is typically 10000 times larger in volume. Even if the nanostructure is ferromagnetic and the substrate only diamagnetic, the correction due to the substrate is in most cases much stronger than the signal itself.

Better adapted to thin structures are methods that are surface sensitive. The magneto-optical Kerr effect (MOKE) measures magnetization with polarized light reflected from a magnetic surface. Due to the magnetization of the sample the polarization direction of the light is modified. This method is surface sensitive in the range of the penetration depth of the light used (typically some 10 nanometers). At synchrotron x-ray sources one can use X-ray Magnetic Circular Dichroism (XMCD). The energy dependence of the absorption of circular polarized (soft) x-rays is measured at the absorption edges of the magnetic materials. Again, the information is integrated over the penetration depth of the x-rays used, but it is element specific due to the choice of the x-ray energy in resonance with the magnetic orbitals of a certain element.

Magnetic domains can be imaged using e.g. Magnetic Force Microscopy (surface sensitive, measuring the stray fields above the sample), Lorentz microscopy (the transmission of electrons through a very thin sample is observed; due to the Lorentz forces the electrons are deviated according to the magnetization strength and direction), or Kerr microscopy (observing the MOKE using an optical microscope; again it integrates over the penetration depth of the light, with the lateral resolution of the optical microscope). Photoemission electron microscopy (PEEM) with soft x-rays can give an overview about the density of certain electronic states with a lateral resolution in the nanometer range and time resolution down to nanoseconds. In combination with XMCD, XMCD-PEEM can visualize the evolution of magnetic domains under variable magnetic fields. But again, the depth resolution is only determined by the penetration depth and the element specific absorption of the x-rays.

What is missing is a method that can access the magnetism of buried layers using the depth information. Here, we need a probe that is sensitive to magnetic fields while having a spatial resolution (at least in depth) in the nm regime. Cold neutrons have a wavelength appropriate for resolving nm length scales and they carry a spin that interacts with the magnetic fields. For most of the magnetic investigations, the neutron's

spin has to be prepared in a certain state, so we use polarized neutrons for the investigation of magnetic nanostructures.

Polarized neutron reflectometry with polarization analysis is a method for depth-resolved investigation of magnetic layered structures; I will introduce this method in the following chapter. Together with the analysis of off-specular scattering, lateral structures in the μm range can be investigated, allowing to access magnetic domains in buried layers. Polarized SANS reveals information about magnetic structures in the nm range perpendicular to the beam direction, while polarized GISANS (Grazing Incidence Small Angle Neutron Scattering) combines the possibilities of both methods and allows to access lateral magnetic structures in the nm range in buried layers.

10.3 Specular reflectivity of polarized neutrons

In the previous lecture, you have learned about specular reflectivity of neutrons on layered structures with nuclear scattering contrast. For the investigation of magnetic layered structures, we have to remind that the neutron is a spin $\frac{1}{2}$ particle and therefore interacts with the magnetic induction \mathbf{B} .

To treat the neutron's spin properly, we have to work with wave functions in the 2-dimensional quantum mechanical spin space, where the usual space-dependent functions, e.g. the potential, become operators on the neutron's spin.

In analogy to eq. (9.2), the potential of a homogeneous magnetic material can be separated into two parts

$$\hat{V}_1 = V_1^N \hat{1} + \hat{V}_1^M \quad (10.1)$$

where V_1^N is the nuclear interaction from eq. (9.2), and $\hat{1}$ is the unity operator, which does not affect the spin state, so that the nuclear interaction is described independently on the neutron's spin. The magnetic dipole interaction is described by the operator $\hat{V}_1^M = -\mu_n \hat{\boldsymbol{\sigma}} \cdot \mathbf{B}_1$ which is a scalar product of the neutron magnetic moment operator $\mu_n \hat{\boldsymbol{\sigma}}$ and the magnetic induction \mathbf{B}_1 inside the material.

For the description in coordinates, we need to define a coordinate system which is convenient to describe the experiment. Typically, the magnetic field \mathbf{H} is applied in the plane of the sample. We choose this direction to be the x-direction of the coordinate system $\mathbf{H} = H \mathbf{e}_x$ and also as the quantization axis for the neutron spin. Under this assumption, the spin operator $\hat{\boldsymbol{\sigma}} = (\sigma_x, \sigma_y, \sigma_z)$ is the following:

$$\sigma_x = \begin{pmatrix} 1 & 0 \\ 0 & -1 \end{pmatrix} \quad \sigma_y = \begin{pmatrix} 0 & 1 \\ 1 & 0 \end{pmatrix} \quad \sigma_z = \begin{pmatrix} 0 & -i \\ i & 0 \end{pmatrix} \quad (10.2)$$

In analogy to chapter 9.2, the Schrödinger equation can be solved in coordinate and spin space, where the eigenvectors $|+\rangle$ and $|-\rangle$ of the operator $\hat{\sigma} \cdot \mathbf{b}_0 = \sigma_x$ with the eigenvalues +1 and -1, respectively, define states of the neutron with “spin up” and “spin down”. The solution of the Schrödinger equation is the neutron wave function $|\Psi(\mathbf{r})\rangle$, which is again a linear combination of those two spin states.

$$|\Psi(\mathbf{r})\rangle = \Psi^+(\mathbf{r})|+\rangle + \Psi^-(\mathbf{r})|-\rangle = \begin{pmatrix} \Psi^+(\mathbf{r}) \\ \Psi^-(\mathbf{r}) \end{pmatrix} \quad (10.3)$$

After some calculation which you can find in Ref [6] we end up with a set of two coupled one-dimensional linear differential equations for every layer, which are the analogue to equation (9.8).

$$\Psi_1^{+''}(z) + [k_{z1}^2 - 4\pi(\rho_1^N + \rho_1^M m_{x1})]\Psi_1^+(z) - 4\pi\rho_1^M m_{y1}\Psi_1^-(z) = 0 \quad (10.4)$$

$$\Psi_1^{-''}(z) + [k_{z1}^2 - 4\pi(\rho_1^N - \rho_1^M m_{x1})]\Psi_1^-(z) - 4\pi\rho_1^M m_{y1}\Psi_1^+(z) = 0 \quad (10.5)$$

In this formulae, you find the nuclear scattering length density ρ^N that you know from eq. (9.3) together with its magnetic analogon ρ^M , the magnetic scattering length density. It is proportional to the net magnetization M of the material. In case of a ferromagnetic material, the magnetization vector \mathbf{M} typically is aligned in some direction, which is described by the unit vector $\mathbf{m} = \mathbf{M} / M$.

Now, we can have a closer look at the different terms in equation (10.4) and (10.5). As Non-Spinflip (NSF) interaction, one finds in (10.4) for spin + (“spin up”) the sum of the nuclear interaction and the magnetic interaction with the magnetization along the quantization direction and in (10.5) for spin – (“spin down”) the difference. In case of a magnetically saturated layer (all the magnetization is aligned with the external field), the scattering length density for spin + neutrons is enhanced and for spin – neutrons is reduced compared to the nonmagnetic case.

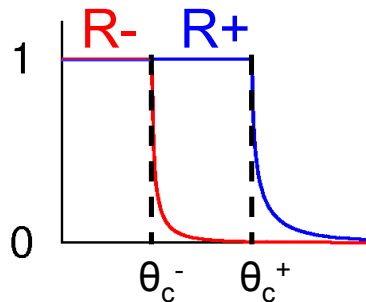


Fig. 10.5: *The total reflection angle θ_c of the surface of a magnetized material is different for both spin directions*

This has an influence on the index of refraction, on the total reflection angle, and of course on the reflectivity, which is a function of the change of the index of refraction at a certain interface. Fig. 10.5 shows schematically the splitting of the total reflection angle.

In case that the magnetization is not fully aligned with the field, the component along the field direction influences the scattering length density for NSF. The in-plane magnetization component perpendicular to the field induces a spin-flip (SF) interaction that is equally strong for both spin-flip channels $+ -$ and $- +$, as is described in the last term of eq. (10.5) or (10.4), respectively.

Specular reflectivity of polarized neutrons is not sensitive to any magnetization component perpendicular to the layer plane. This is in agreement with the statement in lecture 7 (eq. (7.17) ff.) that only the magnetization component \mathbf{M}_\perp perpendicular to \mathbf{Q} contributes to the magnetic interaction with the neutron's spin.

As an example, I would like to show the polarized neutron reflectivity of a [Co / Cu] multilayer. The respective nuclear and magnetic scattering length densities are

$$\begin{aligned} \text{Co: } \rho_N &= 2.30 \cdot 10^{-6} \text{ \AA}^{-2} & \rho_M &= 4.24 \cdot 10^{-6} \text{ \AA}^{-2} \\ \text{Cu: } \rho_N &= 6.53 \cdot 10^{-6} \text{ \AA}^{-2} & \rho_M &= 0. \end{aligned}$$

Obviously, the sum of the magnetic and the nuclear scattering length density of Co is almost equal to the scattering length density of Cu. In the case of magnetic saturation, spin + neutrons will not feel any contrast at the Co / Cu interfaces because they see the sum of nuclear and magnetic scattering length density in the Co layer. The multilayer structure is invisible for spin + neutrons. In contrast, spin - neutrons experience the difference of nuclear and magnetic scattering length density (which is in fact negative), so that the contrast is huge.

Fig. 10.6 makes the contrast situation visible by using colours representing the different scattering length densities.

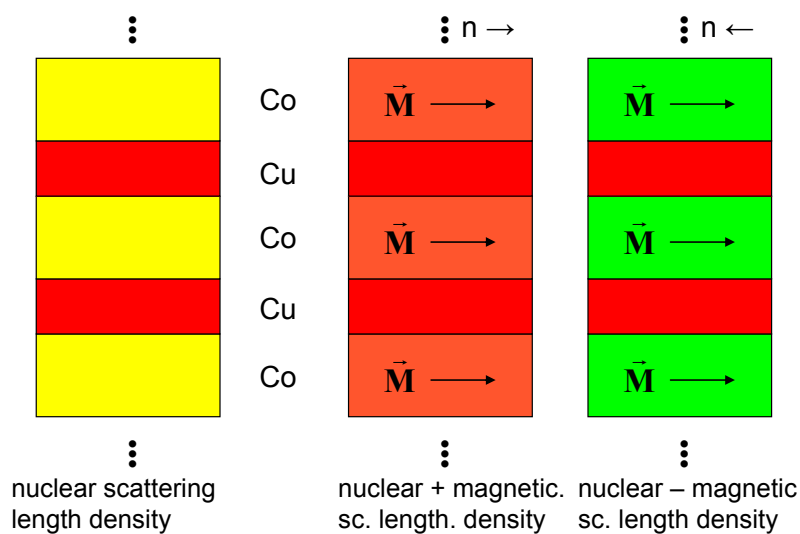


Fig. 10.6: *The contrast between Co and Cu depends on the magnetization state. It almost vanishes for spin up neutrons, but is strong for spin down.*

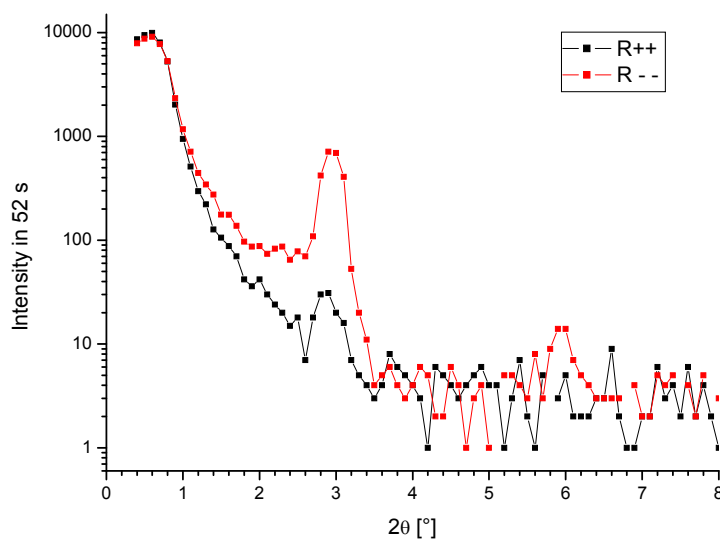


Fig. 10.7: *Specular reflectivity of polarized neutrons from a [Co/Cu] multilayer with 20 periods at magnetic saturation*

Fig. 10.7 shows the measured polarized neutron reflectivity of such a multilayer. The total reflection edge is identical for both spin channels, because the biggest scattering length density in the layered structure is the one of Cu, which is not magnetic. But the multilayer Bragg peaks at $2\theta = 3^\circ$ and $2\theta = 6^\circ$ are strongly spin split. For spin – neutrons, the Bragg peak is about 30 times stronger than for spin + neutrons. Here, one can see that the contrast is responsible for the reflectivity, not the strength of the scattering potential, as the scattering length density (which describes the scattering potential) is higher for spin +, but the contrast between the layers is much stronger for spin –.

10.4 Layer-by-layer magnetometry

One important application of polarized neutron reflectometry with polarization analysis is layer-by-layer magnetometry. As an example, I present the magnetization evolution in exchange bias multilayers of the type $[\text{IrMn} / \text{CoFe}]_N$ with the number of periods [7]. The exchange bias effect is the coupling between a ferromagnetic layer and a neighbouring antiferromagnetic layer. If the antiferromagnet has been cooled below its Néel temperature with the ferromagnet being saturated, it conserves the interface magnetization without being sensitive to the applied magnetic field. This induces an additional unidirectional anisotropy on the ferromagnetic layer, i.e. the original magnetization direction is preferred over all others. The hysteresis loop is shifted away from $H = 0$.

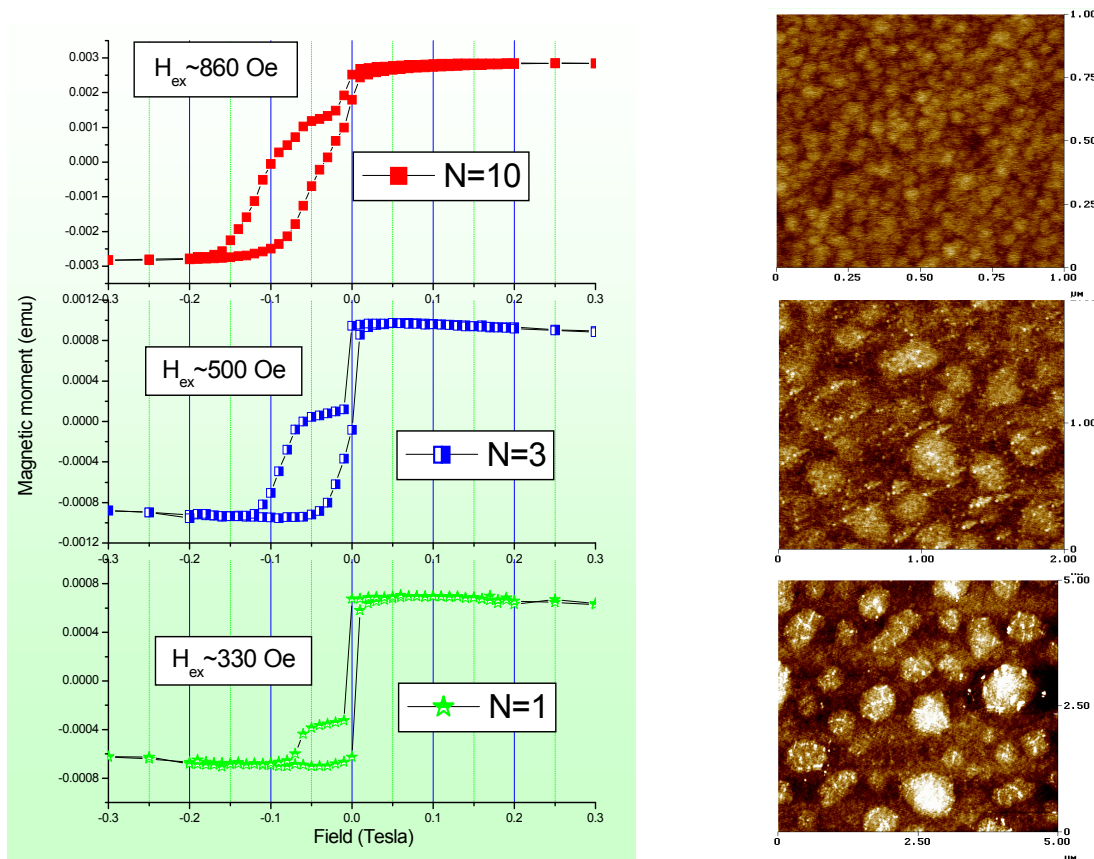


Fig. 10.8: *SQUID magnetization measurements (at room temperature, left) and AFM micrographs of the surface (right) of polycrystalline multilayers of the type $\text{SiO}_2 / 10 \text{ nm NiFe} / [5 \text{ nm IrMn} / 3 \text{ nm CoFe}]_N$ with $N = 1, 3$, or 10 , resp.*

The green curve in Fig. 10.8 shows the exchange biased magnetization curve of a IrMn / CoFe double layer shifted left together with the magnetization loop of the NiFe buffer layer, which is not affected by exchange bias and therefore symmetric around $H = 0$ field. The CoFe layer shows a nice square hysteresis loop, indicating spontaneous magnetization flip at the coercive field.

Strangely, the shape of the magnetization loop of the exchange biased CoFe layers changes, when the number of [IrMn / CoFe] $_N$ bilayers is increased. In addition, the strength of the exchange bias is increased. An AFM study of the surfaces shows that the grain size of the polycrystalline layers is reduced from layer to layer during the preparation procedure, but no information could be found that justifies the slope of the magnetization curves and that could eventually explain the origin of a magnetization rotation process responsible for the gradual evolution of the magnetization as a function of the applied field.

Therefore, a polarized neutron reflectivity study was performed, to investigate the individual behaviour of the ferromagnetic layers in the multilayer structure. As an example, Fig. 10.9 shows the specular polarized neutron reflectivity at one of the coercive fields (i.e. the net magnetization vanishes) together with the fit.

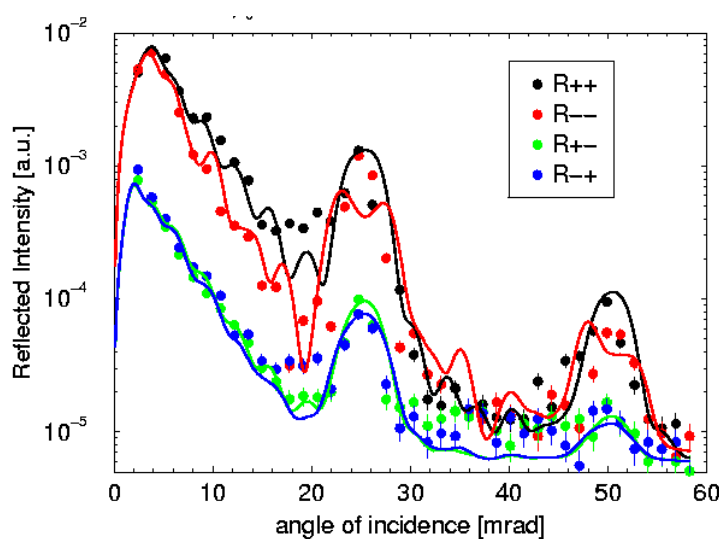


Fig. 10.9: Polarized neutron reflectivity of the sample with $N=10$ at $\mu_0 H = -0.1$ mT after positive saturation

The polarized neutron measurement shows no spin flip signal at all, immediately excluding the idea of a magnetization rotation process. Furthermore, the fit of the measured data shows that the magnetization of the upper 5 CoFe layers is aligned antiparallel to the field while the magnetization of the lower 5 CoFe layers is still aligned along to the field. I.e., the exchange bias on the upper layers (with smaller grains) still can hold the magnetization in the preferred direction, while the magnetization of the lower layers already has followed the field.

Together with measurements at several other magnetic field values on both branches of the hysteresis loop it turned out that every single layer has a square magnetization loop, but the strength of the exchange bias effect (i.e. the shift of the centre of the loop away from $H = 0$) increases with reduced grain size. The overlaying of the differently shifted square loops then results in the inclined net magnetization loop measured with magnetometry.

10.5 Vector magnetometry

The second important application of polarized neutron reflectometry with polarization analysis is vector magnetometry in layered structures. The ability to distinguish between SF and NSF channels offers an independent access to the in-plane magnetization components perpendicular and parallel to the field direction. As a magnetization direction perpendicular to the sample surface is rare (due to the shape anisotropy) one can determine the full magnetization vector in most cases.

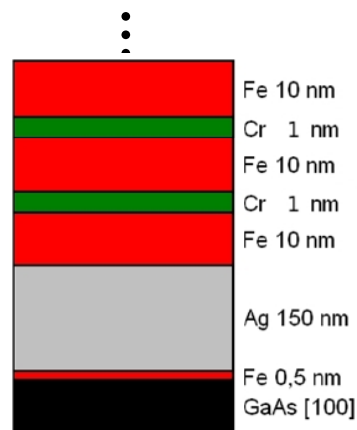


Fig. 10.10: Layer sequence of an epitaxially grown and antiferromagnetically coupled $[Fe / Cr]_N$ multilayer

I would like to explain the power of vector magnetometry using the example of an epitaxially grown and antiferromagnetically (AF) coupled $[Fe / Cr]_N$ multilayer with an odd number of Fe layers [8]. Fig. 10.10 shows the layer sequence of such a sample grown on a GaAs single crystal with a Ag buffer layer to improve the surface quality. The magnetic behaviour is determined by the competition between 3 different interactions (see.

Fig. 10.11): The crystalline anisotropy in the single crystalline Fe layers tries to align the magnetization in every Fe layer along one of the in-plane $[100]$ directions. This results in 4 equivalent easy axes. The antiferromagnetic coupling (mediated by the Cr interlayer) has the tendency to align the magnetization of two neighbouring Fe layers antiparallel to each other. The Zeeman term tries to align the magnetization of every ferromagnetic layer along the applied field.

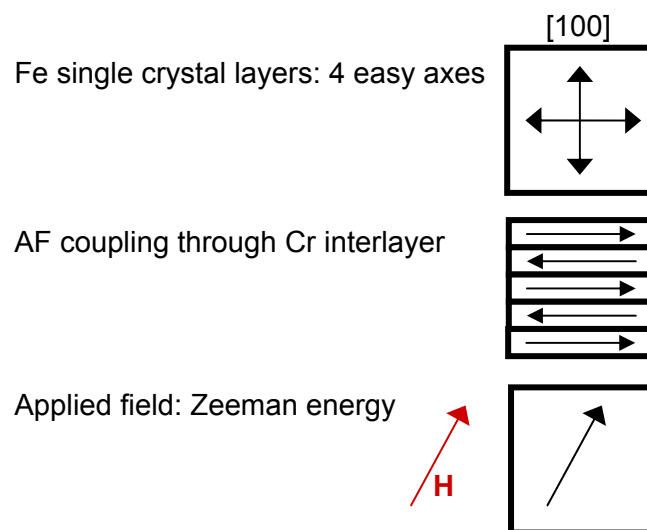


Fig. 10.11: *The magnetic behaviour in an applied magnetic field is governed by 3 competing interactions*

As the multilayer under investigation has an odd number of Fe layers, the antiparallel orientation of the magnetization in remanence (where the Zeeman term is weak) will leave the magnetization of one layer uncompensated, so that the Zeeman energy does not vanish even at very small fields. This effect is supposed to align the remanent magnetization of all layers along or antiparallel to the field direction.

Fig. 10.12 shows MOKE measurements of such samples with $N = 7$ or $N = 19$ Fe layers in the multilayer sequence. The MOKE signal is a function of the magnetization, but not proportional to it, because it is a superposition of the longitudinal Kerr effect (proportional to the magnetization along the field) and the transverse Kerr effect (proportional to the magnetization perpendicular to the field). Furthermore, the weight of the layers close to the surface is much higher than the weight of lower lying layers due to the limited penetration depth of the light. Therefore, one should not worry about the MOKE curve not being monotonous. Nevertheless, a jump in the MOKE curve always indicates a spontaneous change of the magnetization state.

In addition, Fig. 10.12 shows a simulation of the integral magnetization component along the field based on a numerical minimization of the three energy terms mentioned above. This kind of simulation cannot reproduce effects of activation barriers leading to hysteresis.

In the case of the multilayer with $N = 7$ Fe layers, the simulation and the MOKE measurement have a good qualitative agreement. In saturation, the magnetic moment of every layer is aligned with the field. In the intermediate field range, the magnetization is alternately pointing left or right from the field direction, so that the magnetization component along the field is almost equal for every layer and the magnetization components perpendicular to the field fulfil as much as possible the AF coupling.

At remanence, the magnetization of all layers is turned by 90° , so that 4 layers have the magnetization along the field and 3 layers antiparallel to the field. This configuration fulfils as well the AF coupling condition as the alignment of the net magnetization along the applied field.

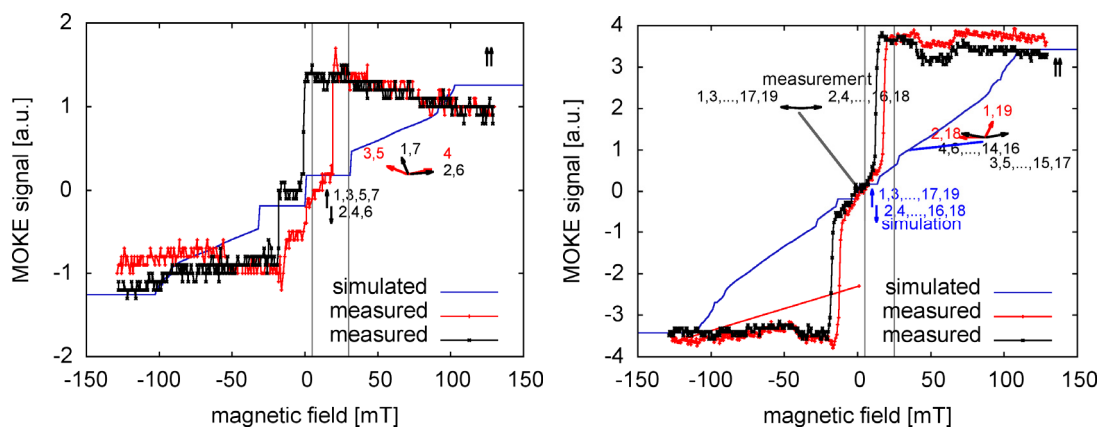


Fig. 10.12: *MOKE measurement of $[Fe / Cr]_N$ multilayers with $N = 7$ Fe layers (left) and $N = 19$ Fe layers (right). The simulation of the magnetization curve is based on minimization of the total energy.*

In contrast to that, the MOKE measurement of the multilayer with $N = 19$ Fe layers shows a smooth transition through $H = 0$ while the simulation proposes a step comparable to the case described previously. This behaviour is known from AF coupled multilayers with an even number of ferromagnetic layers, because there the net magnetization vanishes, so that there is no Zeeman energy that causes the rotation of the entire magnetic configuration at remanence. This contradiction cannot be resolved by magnetometry measurements only.

Fig. 10.13 shows the polarized neutron reflectivity together with the offspecular scattering for the two samples at saturation field. One can see a structured signal with total reflection and several Bragg peaks according to the periodicity in the multilayer structure only in the R_{++} channel. For spin $-$ neutrons the contrast between fully magnetized Fe and Cr vanishes, so the R_{--} shows only the total reflection (with a reduced critical angle compared to R_{++}), but no Bragg peaks. As no magnetization component perpendicular to the field direction exists, there is no real spin flip signal. What you see in R_{+-} and R_{-+} is a parasitic signal due to the limited efficiency of the polarizing equipment of the instrument. The Bragg sheets crossing the specular Bragg peaks are due to vertically correlated roughness of the Fe / Cr interfaces.

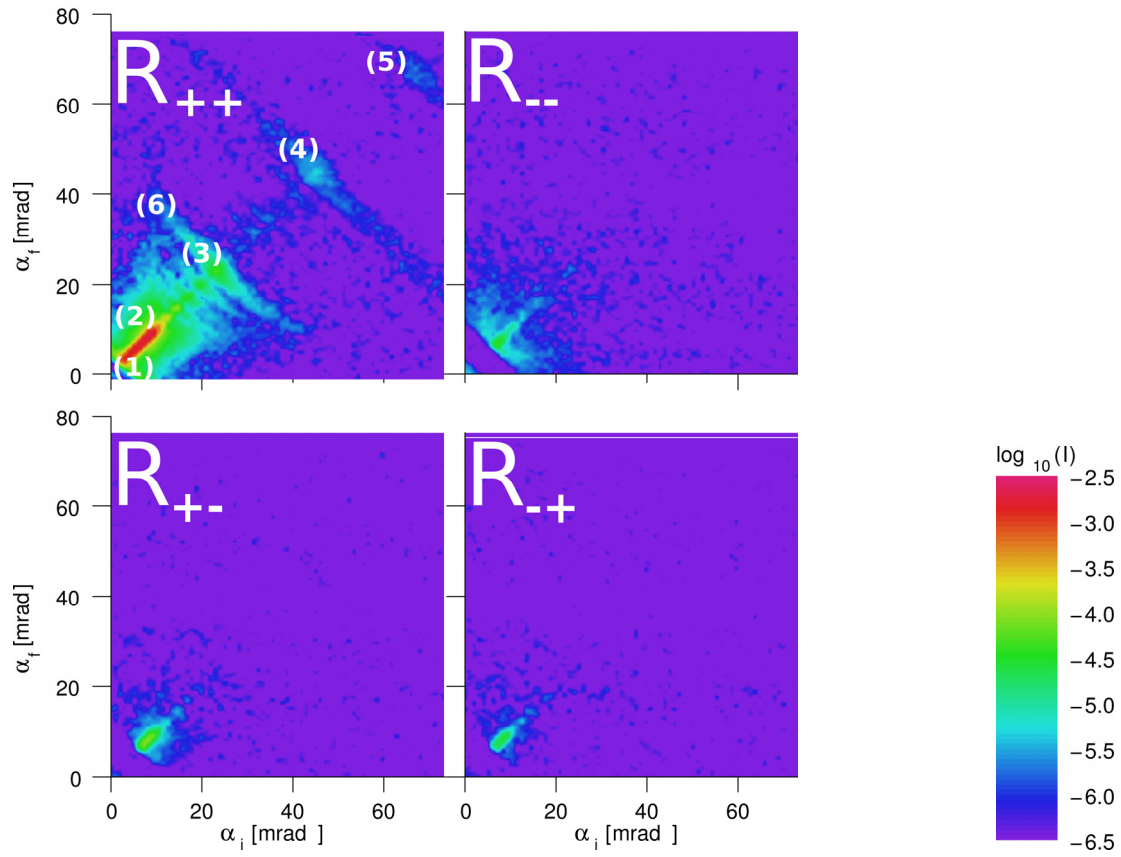
No qualitative difference between the two samples can be observed except the fact that the Bragg peaks and Bragg sheets are sharper and more intense for the $[Fe / Cr]_{19}$ sample because of the bigger number of periods.

Fig. 10.14 shows the same in the intermediate field range. Additional Bragg peaks of half order appear, which are stronger in SF compared to NSF. This is the indication of the alternation of the magnetization directions due to the antiferromagnetic coupling. Mainly the magnetization component perpendicular to the field oscillates while the component remaining along the field is modulated less. As the sample is no more saturated, the magnetization component in field direction is reduced, so that the contrast for spin $-$ neutrons does not vanish any more. Therefore, the full order Bragg peaks also come up in R_{--} . They are now mainly induced by the nuclear structure while the magnetic contribution is collected in the half order signal. The strong off-specular signal around the half order Bragg peaks in the SF channels is a signature of magnetic domains. Again, no distinct qualitative difference between the two samples is observed.

This is very different at remanence, as shown in Fig. 10.15. The $[Fe / Cr]_7$ sample has all half order peaks in the NSF channels while the $[Fe / Cr]_{19}$ sample has all half order peaks in SF. The small contribution in the other channels can be explained due to the limited polarization of the neutron beam. This shows that the magnetization of all layers of the $[Fe / Cr]_7$ sample is aligned alternately parallel and antiparallel to the field direction, as has been proposed by the simulation for the MOKE measurement.

In the case of the $[Fe / Cr]_{19}$ sample, all magnetization is now concentrated perpendicular to the field, no more difference between R_{++} and R_{--} can be observed. The measurement clearly shows that the Zeeman energy contribution equivalent to the magnetization of a single Fe layer is not sufficient to turn the entire magnetization of all 19 layers by 90° across the crystalline anisotropy barrier.

In addition to the qualitative description presented here, a quantitative analysis of the measurements allows to determine the angle of the magnetization vector of every layer independently. This analysis is presented in Ref. [8].



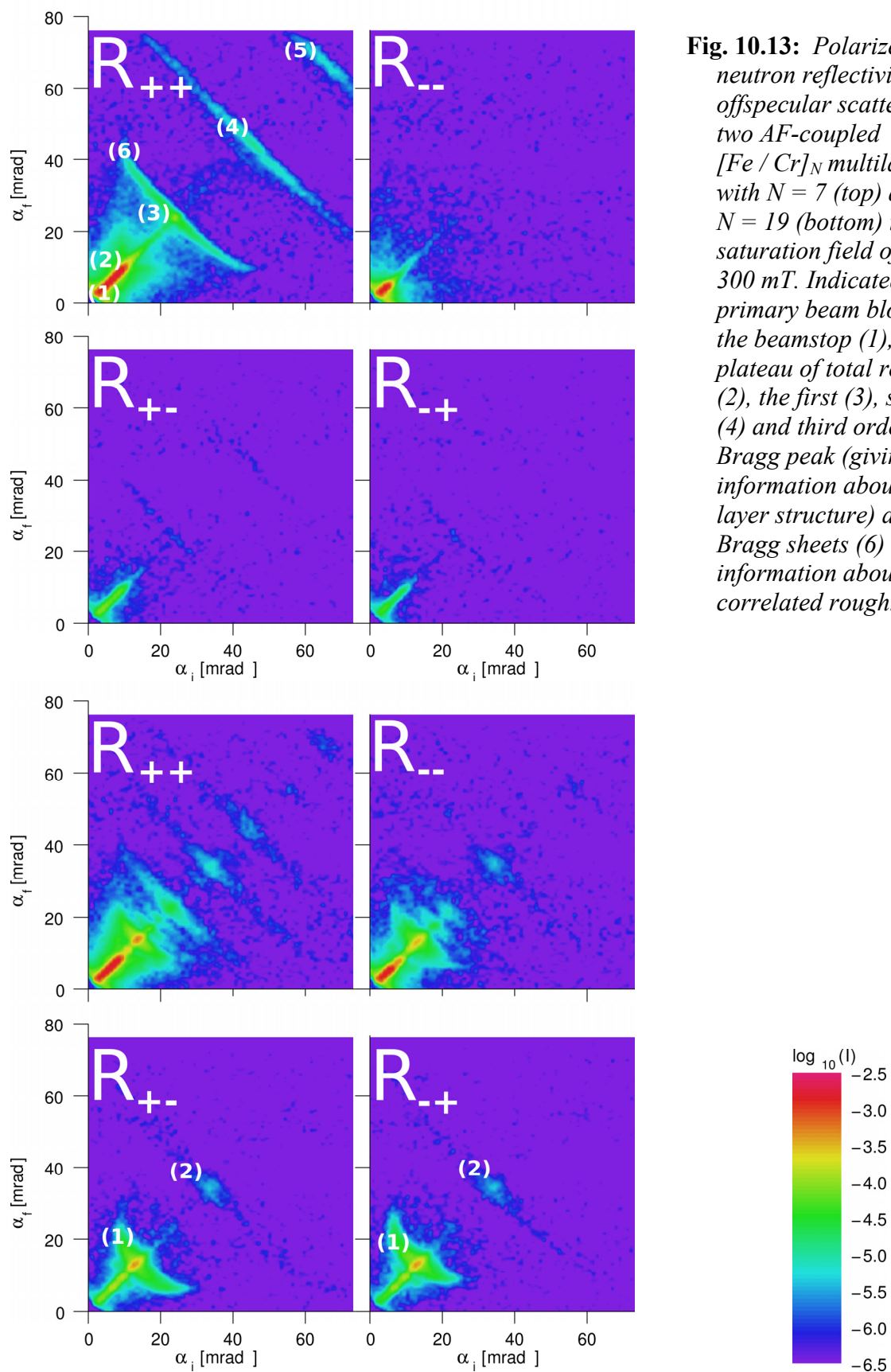


Fig. 10.13: Polarized neutron reflectivity and offspecular scattering for two AF-coupled $[\text{Fe}/\text{Cr}]_N$ multilayers with $N = 7$ (top) and $N = 19$ (bottom) in saturation field of 300 mT. Indicated are the primary beam blocked by the beamstop (1), the plateau of total reflection (2), the first (3), second (4) and third order (5) Bragg peak (giving information about the layer structure) and the Bragg sheets (6) (giving information about correlated roughness).

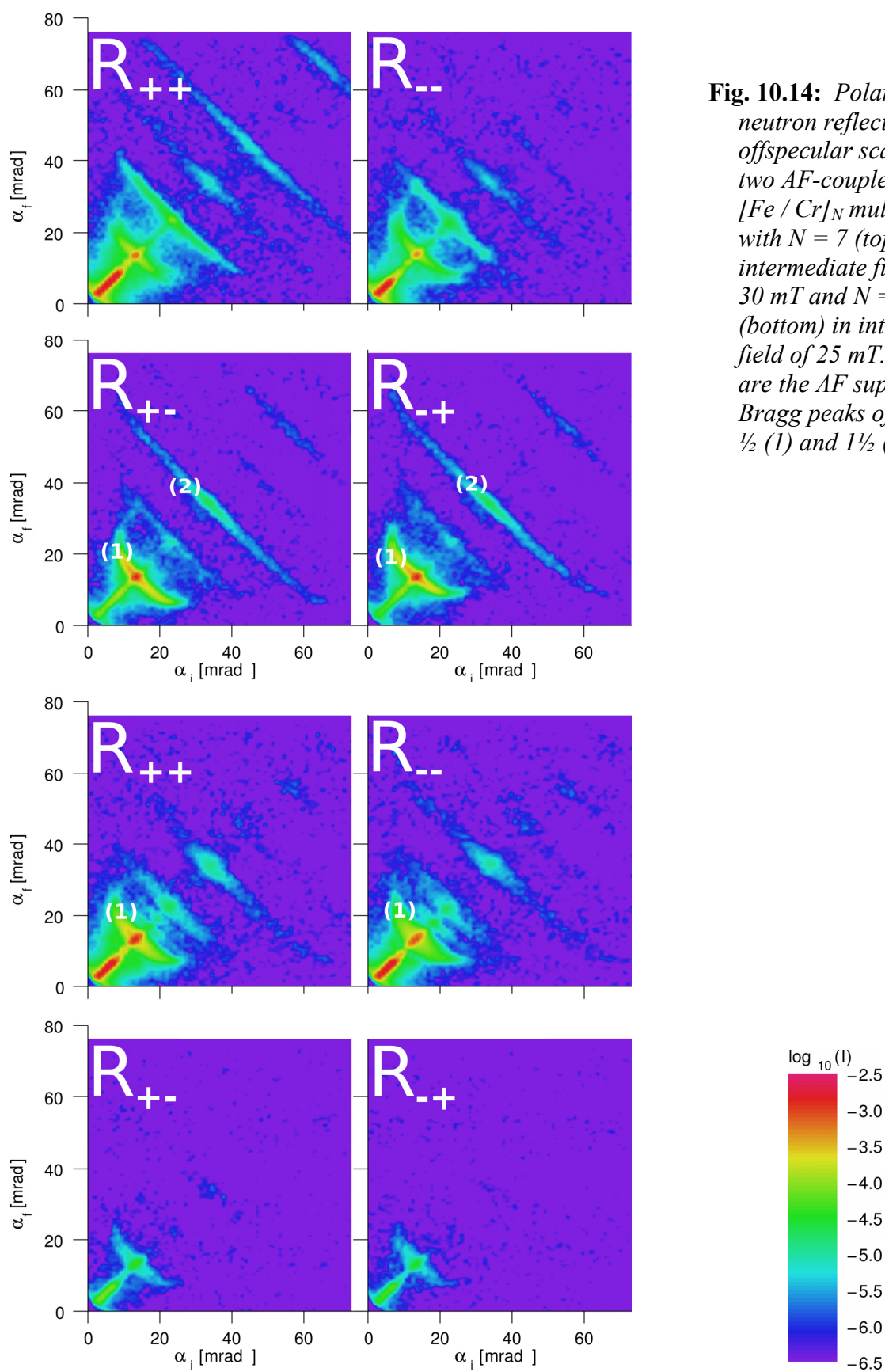


Fig. 10.14: Polarized neutron reflectivity and offspecular scattering for two AF-coupled $[Fe/Cr]_N$ multilayers with $N=7$ (top) in intermediate field of 30 mT and $N=19$ (bottom) in intermediate field of 25 mT. Indicated are the AF superstructure Bragg peaks of the order $\frac{1}{2}$ (1) and $1\frac{1}{2}$ (2).

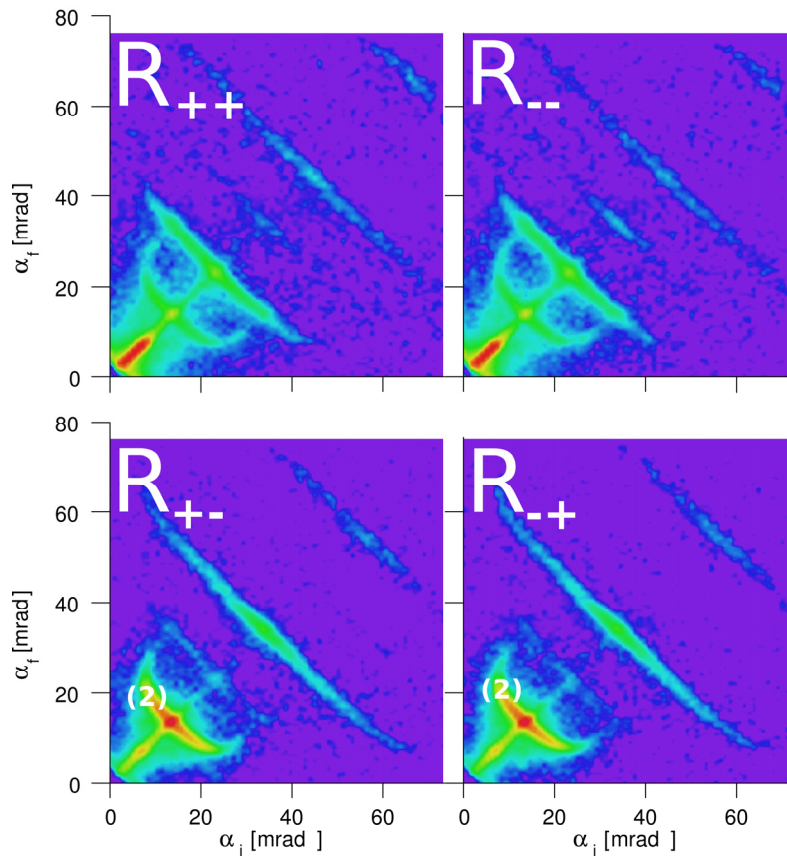


Fig. 10.15: Polarized neutron reflectivity and offspecular scattering for two AF-coupled $[\text{Fe} / \text{Cr}]_N$ multilayers with $N = 7$ (top) and $N = 19$ (bottom) in remanence field of 5 mT. Indicated are the AF superstructure Bragg peaks of order $\frac{1}{2}$ in the NSF channels of the $[\text{Fe} / \text{Cr}]_7$ system (1) and in the SF channels of the $[\text{Fe} / \text{Cr}]_{19}$ system (2).

References

- [1] P. Grünberg, R. Schreiber, Y. Pang, M.B. Brodsky, and H. Sowers, *Phys. Rev. Lett.* **57** (1986), 2442
- [2] P.H. Dederichs, “Interlayer Exchange Coupling“, chapter C 3 in “Magnetism goes Nano“, 36th IFF Spring School, Forschungszentrum Jülich, series Matter and Materials, Vol. 26 (2005)
- [3] G. Binasch, P. Grünberg, F. Saurenbach, and W. Zinn, *Phys. Rev. B* **39** (1989), 4828
- [4] M.N. Baibich, J.M. Broto, A. Fert, F. Nguyen Van Dau, F. Petroff, P. Etienne, G. Creuzet, A. Friedrich, and J. Chazelas, *Phys. Rev. Lett.* **61** (1988), 2472
- [5] D.E. Bürgler, “Spin-Transport in Layered Systems“, chapter E 5 in “Magnetism goes Nano“, 36th IFF Spring School, Forschungszentrum Jülich, series Matter and Materials, Vol. 26 (2005)
- [6] U. Rücker, E. Kentzinger, “Thin Film Systems: Scattering under Grazing Incidence“, chapter D4 in “Probing the Nanoworld“, 38th IFF Spring School, Forschungszentrum Jülich, series Matter and Materials, Vol. 34 (2007)
- [7] A. Paul, E. Kentzinger, U. Rücker, D.E. Bürgler, and P. Grünberg, *Phys. Rev. B* **70** (2004), 224410
- [8] E. Josten, U. Rücker, S. Mattauch, D. Korolkov, A. Glavic, and Th. Brückel, *J. Phys: Conf. Ser.* **211** (2010), 012023

Exercises

E10.1 Magnetic contrast

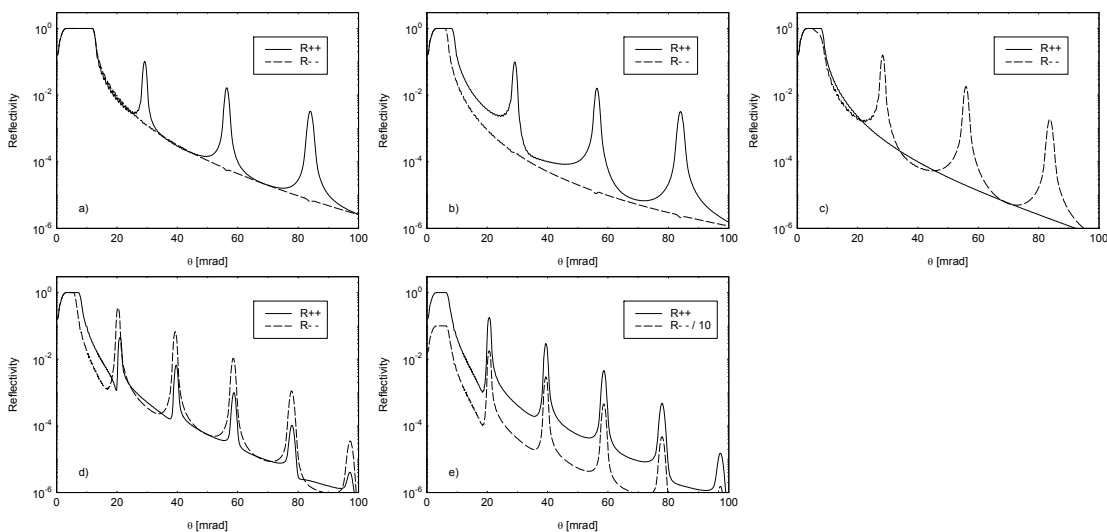
We measure the polarized neutron reflectivity of a $[\text{Ni}_2\text{Fe} / \text{Pt}]_N$ multilayer structure in magnetic saturation. The Ni_2Fe alloy is ferromagnetic.

- a) Calculate the nuclear and magnetic scattering length densities for the two constituents of the multilayer:

	Ni	Fe	Pt
density [g/cm^3]	8.90	7.86	21.4
atomic weight [g/mol]	58.71	55.85	195.09
nuclear scattering length [$1\text{E}-14 \text{ m}$]	1.03	0.954	0.95
magnetic scattering length density [$1\text{E}-6 \text{ \AA}^{-2}$]	1.52	5.12	0

If you do not manage to calculate the values properly, you may continue with the tabulated values of the nuclear scattering length densities: Ni: $9.41\text{E}-6 \text{ \AA}^{-2}$, Fe: $8.09\text{E}-6 \text{ \AA}^{-2}$, Pt: $6.29\text{E}-6 \text{ \AA}^{-2}$.

- b) Which of the 5 reflectivity curves presented below is the one measured on this alloy? Think about the critical angle (has to do with the highest scattering length density in all layers) and the contrast between adjacent layers (influences the height of the diffraction peaks) for both spin directions parallel (R_{++}) and antiparallel (R_{--}) to the applied magnetic field (saturation!).



c) The other 4 curves have been measured on different samples. Which curve belongs to which sample?

- I. The sum of nuclear and magnetic scattering length density of the magnetic layers is equal to the nuclear scattering length density of the nonmagnetic layers
- II. The sample contains an additional nonmagnetic layer with a scattering length density higher than the sum of the magnetic and nuclear scattering length densities of Ni_2Fe on top of the $[\text{Ni}_2\text{Fe} / \text{Pt}]_N$ multilayer
- III. No layer is magnetic
- IV. The nuclear scattering length density of the nonmagnetic layers is somewhere between the sum and the difference of nuclear and magnetic scattering length density of the magnetic layers

E10.2 Vector magnetometry

The following figures show polarized neutron reflectivity measurements with polarization analysis from a ferromagnetic single layer on a nonmagnetic substrate. Find out which figure belongs to which magnetization state:

- I. The sample is magnetized perpendicular to the field direction
- II. The sample is magnetized parallel to the field direction
- III. The magnetization of the sample is inclined by 45° against the field direction
- IV. This set of curves is wrong. (Why?)

